Journal of Nanobiotechnology

RESEARCH

Open Access

Binding-driven forward tearing protospacer activated CRISPR-Cas12a system and applications for microRNA detection

Lina Zhao[1†], Xiangyu Deng[2†], Yuqing Li[1], Qing Zhao[1], Lizhu Xiao[1], Jianjiang Xue[2], Anyi Chen[3*], Wei Cheng[4] and Min Zhao[1*]

Abstract

CRISPR-Cas12a system, characterized by its precise sequence recognition and cleavage activity, has emerged as a powerful and programmable tool for molecular diagnostics. However, current CRISPR-Cas12a-based nucleic acid detection methods, particularly microRNA (miRNA) detection, necessitate additional bio-engineering strategies to exert control over Cas12a activity. Herein, we propose an engineered target-responsive hairpin DNA activator (TRHDA) to mediate forward tearing protospacer activated CRISPR-Cas12a system, which enables direct miRNA detection with high specificity and sensitivity. Target miRNA specifically binding to hairpin DNA can drive forward tearing protospacer in the stem sequence of hairpin structure, facilitating the complementarity between crRNA spacer and protospacer to activate Cas12a. Upon the hairpin DNA as input-responsive activator of Cas12a, a universal biosensing method enables the multiple miRNAs (miR-21, let-7a, miR-30a) detection and also has exceptional capability in identifying single-base mismatches and distinguishing homologous let-7/miR-30 family members. Besides, TRHDA-mediated Cas12a-powered biosensing has realized the evaluation of miR-21 expression levels in diverse cellular contexts by intracellular imaging. Considering the easy programmability of hairpin DNA in responsive region, this strategy could expand for the other target molecules detection (*e.g.*, proteins, micromolecules, peptides, exosomes), which offers significant implications for biomarkers diagnostics utilizing the CRISPR-Cas12a system toolbox.

Keywords CRISPR-Cas12a, MicroRNA, Hairpin DNA, Biosensing

†Lina Zhao and Xiangyu Deng contributed equally to this work.

*Correspondence:
Anyi Chen
chenay@cqmu.edu.cn
Min Zhao
zhaomin@cqmu.edu.cn
Full list of author information is available at the end of the article

Graphical abstract

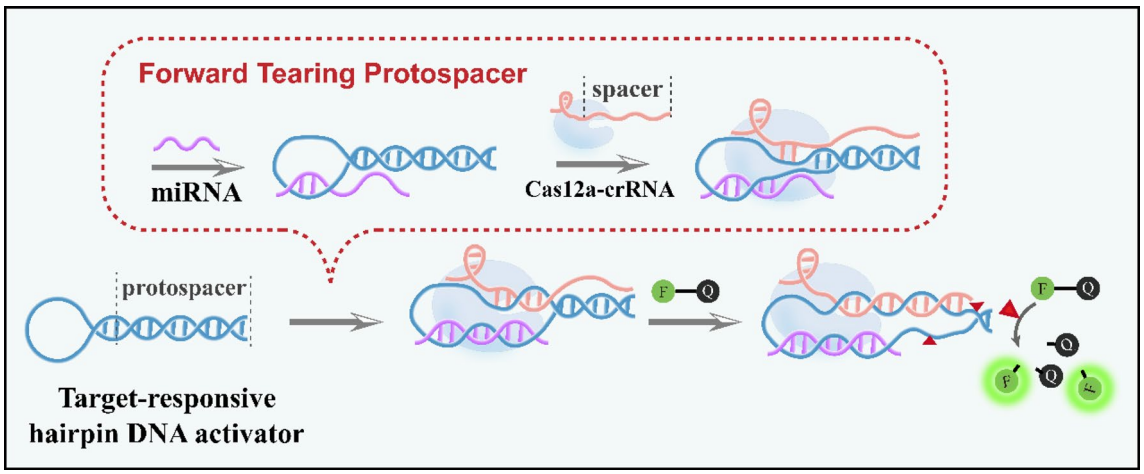

Introduction

MicroRNAs (MiRNAs) belong to a family of small non-coding RNAs, typically ranging from 18 to 24 nucleotides in length, which play crucial roles in the development of human carcinogenesis [1–3]. Multiple investigations have demonstrated that changes in the expression level of miRNAs can provide valuable insights into disease development and progression [4–7]. Nevertheless, the detection of miRNAs poses significant challenges due to their diminutive size, extensive sequence homology within family members, and limited abundance [8, 9]. Currently, the quantification of miRNAs primarily relies on qRT-PCR technology by prior extension of miRNAs into a longer sequence using a stem-loop or tail method because of the characteristics of short miRNA sequence [10, 11]. However, there are numerous limitations associated with challenging primer design, intricate operational procedures, and the requirement for specialized laboratories [12]. Therefore, miRNA detection methods developed on the basis of isothermal nucleic acid amplification, such as rolling circle amplification [13, 14], catalytic hairpin assembly [15, 16], and hybrid chain reaction [17, 18], have attracted extensive research interest as they significantly make miRNA detection simple and feasible. The inclusion of intricate nucleic acid conversion and amplification steps, however, has compromised the specificity of miRNA detection, thereby impeding its practical application in clinical testing. Consequently, the development of simple, specific, and sensitive method for miRNA detection remains an urgent need.

CRISPR-Cas system, an acquired immune system found in prokaryotes, has sparked a remarkable revolution in the field of nano-biotechnology, ranging from genome editing to bio-imaging and in vitro diagnostics due to its programmable capability to precisely cleave nucleic acids at specific target sites [19–22]. Especially, CRISPR-based molecular diagnostics technology has witnessed rapid advancements and also presents exceptional sensitivity and user-friendly operation at point-of-care test, such as DETECTOR [23], SHERLOCK [24], HOLMES [25], etc. Among various CRISPR-Cas systems, Cas12a has been regarded as one of the most powerful and promising nucleic acid recognizers and signal amplifiers, which possesses the ability to recognize and cleave ssDNA or dsDNA targets (cis-cleavage), followed by rapid and indiscriminate cleavage of any nearby ssDNA (trans-cleavage) [26–31]. However, CRISPR-Cas12a activated by ssDNA targets (ssDNA activator) or dsDNA targets (dsDNA activator) has the following characteristics: (i) the specificity of ssDNA-activated Cas12a is weak due to the direct complementarity between crRNA spacer and protospacer on the ssDNA [23] (Scheme 1A); (ii) the universality of dsDNA-activated Cas12a mode is limited owning to the restrictive protospacer adjacent motif (PAM) sites on the dsDNA [32]. Because only upon PAM recognition by Cas12a, can the crRNA spacer hybridize with the protospacer to further activate Cas12a (Scheme 1B). Consequently, aforementioned two Cas12a activation modes emerge technical bottlenecks of the specificity of ssDNA activator and the universality of PAM-dependent dsDNA activator, which restrict Cas12a in the direct detection of nucleic acid targets. In other words, to enable the detection of short RNAs (including miRNAs) using Cas12a, additional bio-engineering strategies such as reverse transcription or nucleic acid amplification are indispensable for converting target nucleic

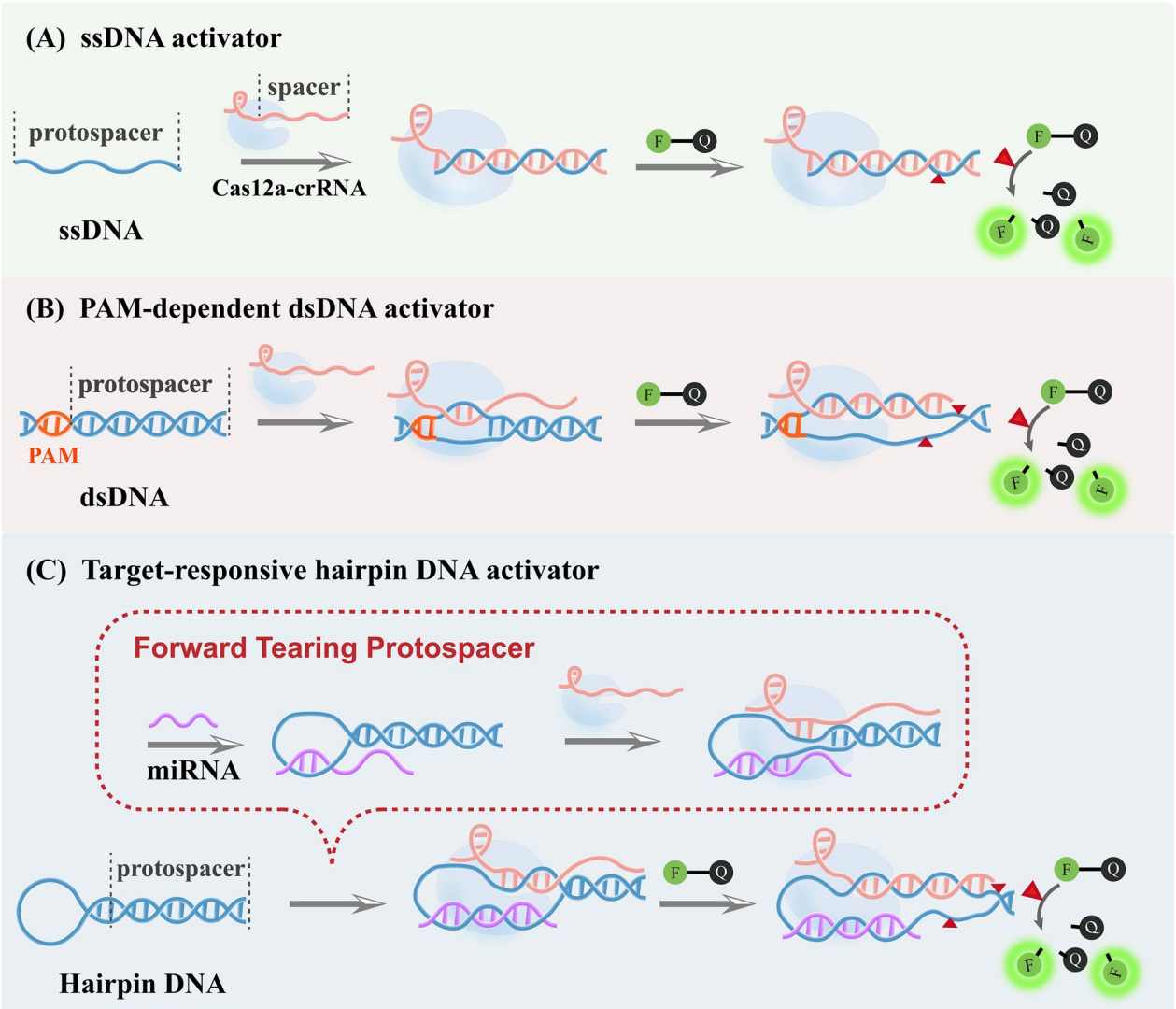

Scheme 1 Schematic illustration of different CRISPR-Cas12a activation modes. **A** SsDNA activator-based Cas12a activation mode. **B** PAM-dependent dsDNA activator-based Cas12a activation mode. **C** Target-responsive hairpin DNA activator (TRHDA)-based forward tearing protospacer induced Cas12a activation mode

acid into ssDNA or dsDNA with PAM sequences to activate Cas12a [33–36]. However, the additional conversion process poses challenges in terms of cost, error rate, time consumption, and operational complexity, which is adverse to the construction of accurate and rapid clinical detection methods. Therefore, it is crucial to develop a streamlined approach utilizing the CRISPR-Cas12a for miRNA detection to meet the demands of clinical diagnostics.

In this work, a novel forward tearing protospacer activated CRISPR-Cas12a system is proposed by utilizing a target-responsive hairpin DNA activator (TRHDA), which is further employed to rapid, one-step detection of miRNA without pre-amplification procedures. As the principle diagram present in Scheme 1C, target miRNA binds to the loop region of hairpin DNA and then extends towards the loop proximal stem region, facilitating forward tearing protospacer in stem sequence of hairpin DNA. This process enables crRNA spacer hybridization with protospacer to form the R-loop, thereby activating the cleavage activities of Cas12a. In the absence of target miRNA, the protospacer in stem sequence of hairpin DNA, which is complemented with crRNA spacer, is sequestered in a "locked" state, making the hairpin DNA incapable of activating Cas12a. In our design, the forward tearing protospacer behavior responsive to target molecules must be engineered so that cleavage activities of Cas12a are activated only upon target-binding guided

hairpin DNA reconfiguration, thereby ensuring the high specificity for miRNA detection. Upon the delicate TRHDA as input-responsive activators, Cas12a-powered miRNA biosensing platform showcases excellent sensitivity without any additional reverse transcription or amplification steps, which enables the quantification of miRNA expression levels in cells through in situ intracellular imaging. As a proof of concept, the proposed Cas12a activation mode supports programmable input-responsive means like targeting-binding, DNA network hybridization or biorthogonal reaction as a driving force to induce forward tearing protospacer behavior, which expands the applications of CRISPR-based techniques in bioanalysis.

Experimental section

In vitro fluorescence measurement

Before use, the hairpin DNA was annealed in a hybridization buffer (1×NEBuffer 3) at 95 ℃ for 5 min and then slowly cooled to room temperature. 2.5 μL of 2 μM Cas12a, 2.5 μL of 2 μM crRNA, 10 μL of 10×reaction buffer, 1 μL of recombinase inhibitor, and 64 μL of RNase-free H_2O were mixed and then incubated at 37 ℃ for 15 min. Next, 10 μL of miRNA with different concentrations, 5 μL of 500 nM hairpin DNA, and 5 μL of 10 μM FQ-labeled ssDNA reporter (F-Q reporter) were added into the above mixture and then incubated at 37 ℃ for 45 min. Subsequently, the reaction system was terminated at 65 ℃ for 10 min. Finally, the fluorescence intensity was recorded on a fluorescence spectrophotometer with excitation at 490 nm and 600 V.

Polyacrylamide gel electrophoresis

10% native polyacrylamide gel electrophoresis (PAGE) was prepared to verify trans-cleavage activity of Cas12a in the presence of miRNA, resulting in cleavage of reporter 2. Electrophoresis was carried out in 1×TBE buffer (2 mM EDTA, 89 mM tri-boric acid, pH 8.3) for 45 min at 100 V constant pressure on an electrophoresis analyzer (Bio-Rad, USA). Then, the gel was immersed in freshly prepared staining solution (60 mL of 1×TBE buffer containing 3 μL of GelRed) and stained by shaking for 15 min. The gel was scanned with the ChemiDoc XRS system (Bio-Rad, USA).

Cell culture

In addition to MCF-10A (healthy human breast epithelial) cells cultured in specialized medium, HeLa (Human cervical cancer) cells, HepG2 (human hepatocellular carcinoma) cells, and MCF-7 (human breast cancer) cells were cultured in DMEM medium containing 10% fetal bovine serum, 1% streptomycin, and 1% penicillin at 37 ℃ and 5% CO_2, 90% humidity.

Laser scanning confocal imaging

Cells of interest with exponential growth were collected by centrifuging at 800 rpm for 2 min, and then washed twice with 1×phosphate buffer (PBS). A small number of centrifuged cells were seeded on cell slides in 24-well microplate and then cultured at 37 ℃ for 24 h. Next, the cells were fixed in 4% paraformaldehyde at room temperature for 10 min and washed three times with 1×PBS. After fixation, cells were permeabilized with 0.5% v/v Triton-X 100 for 5 min at 37 ℃, and then washed with PBS for 3 times. 10 μL of reaction solution containing 1×NEBuffer 3.0, 4 U RNase inhibitor, 150 nM Cas12a, 150 nM crRNA, 75 nM hairpins and 1.5 μM ssDNA-FQ were added into the surface of the slide attached to the cells and incubated at 37 ℃ for 2 h. After washing with 1×PBS, 4′, 6-diamino-2-phenylindole (DAPI) solution was added for nuclear staining for 10 min, and then the fluorescence of the cells was observed by TCSSP8 confocal scanning system. The fluorescence intensity of each group of cells was quantitatively measured by Image J software. The data represented the normalized average strength value of n cells in each group relative to the experimental group. The excitation optical channels used were 405 nm (DAPI, blue) and 488 nm (FAM, green).

Total miRNA extraction and quantitative reverse transcription polymerase chain reaction (qRT-PCR)

Total miRNAs were extracted from MCF-7, HepG2, HeLa, and MCF-10A cells using miRNA Extraction Kit (Tissue & Cell) (HaiGene Biotech Co., Ltd., China). Total miRNA concentration was determined by NanoDrop 1000 spectrophotometer (Thermo Scientific, USA).

To perform qRT-PCR analysis of miR-21 expression levels, cDNA samples were synthesized by reverse transcription of total miRNA using All-In-One cDNA Synthesis Kit (Applied Biological Materials Inc., Canada). PCR was performed using Blas Taq TM 2X qPCR Master Mix (Applied Biological Materials Inc., Canada) kit on CFX96 Touch Real-Time PCR Detection System (Bio-Rad, USA). Specifically, 2 μL of cDNA sample, 0.5 μL of forward primer (10 μM), 0.5 μL of reverse primer (10 μM), 10 μL of BlasTaqTM2XqPCR MM1 premix, and 7 μL RNase free water were mixed and then performed PCR on 40 cycles at 95 ℃ for 3 min, 95 ℃ for 15 s, and 60 ℃ for 1 min, respectively.

Molecular dynamics simulation

Molecular dynamics simulations of Cas12a-crRNA-miRNA-hairpin DNA system were performed using GROMACS 2021.5 package. Cas12a was parameterized

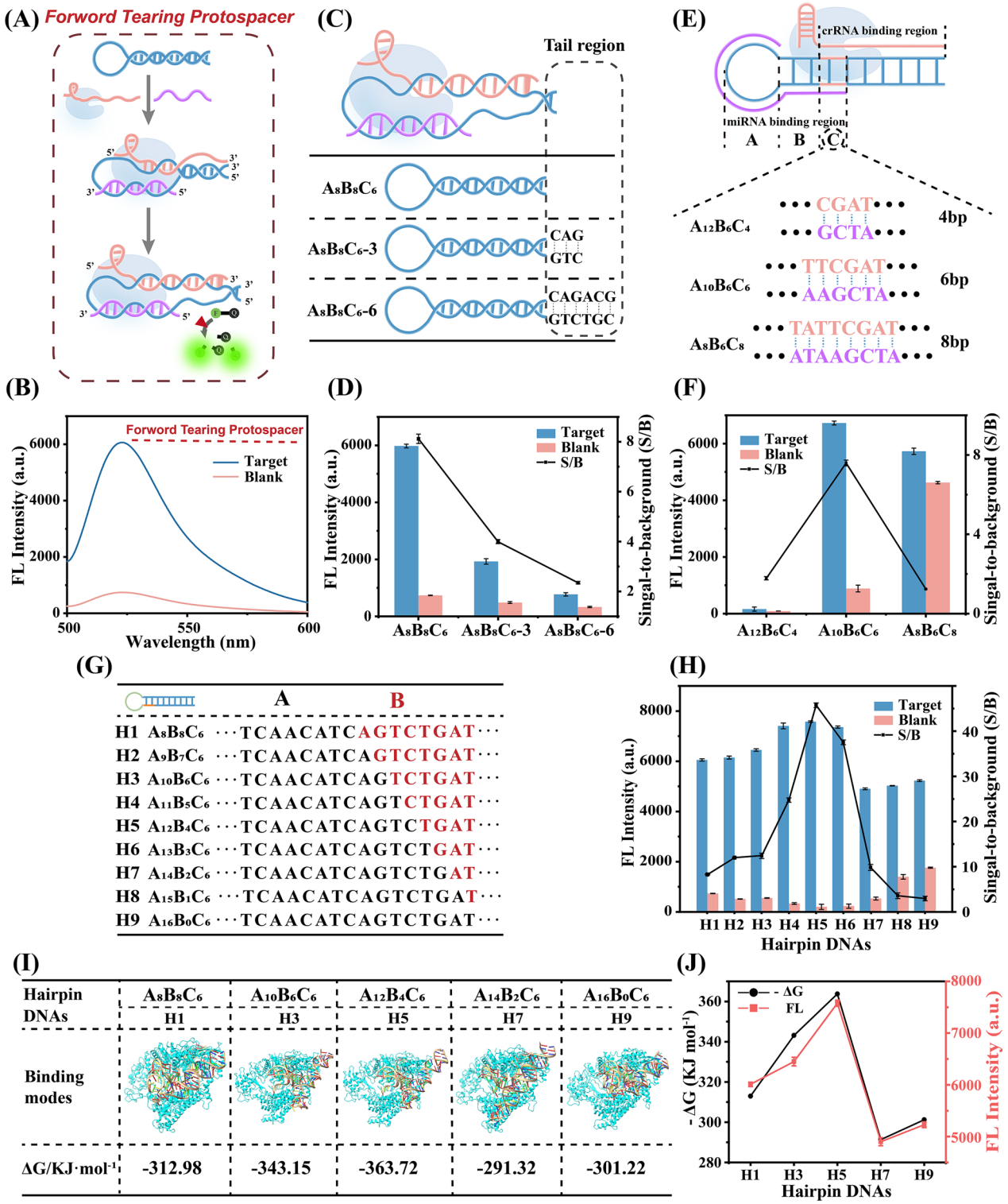

Fig. 1 **A** Schematic illustration and **B** feasibility of TRHDA-based forward tearing protospacer activated Cas12a. **C** Schematic diagram and **D** optimization of the base pair numbers in the tail region of hairpin DNA. **E** Schematic diagram and **F** optimization of the base pair numbers in the "C" region of hairpin DNA. **G** Schematic diagram and **H** parallel optimization of the base pair numbers in "A" region and "B" region of hairpin DNAs (H1 → H9). **I** Molecular dynamics simulations of Cas12a-crRNA-miRNA complex binding to representative five hairpin DNAs (H1, H3, H5, H7, and H9) and the corresponding binding free energies (Δ*G*, KJ·mol^{-1}). **J** Plot of the binding free energy changes *vs.* fluorescence signal changes for five hairpin DNAs (H1, H3, H5, H7, and H9). The data error bars indicate mean ± SD ($n = 3$)

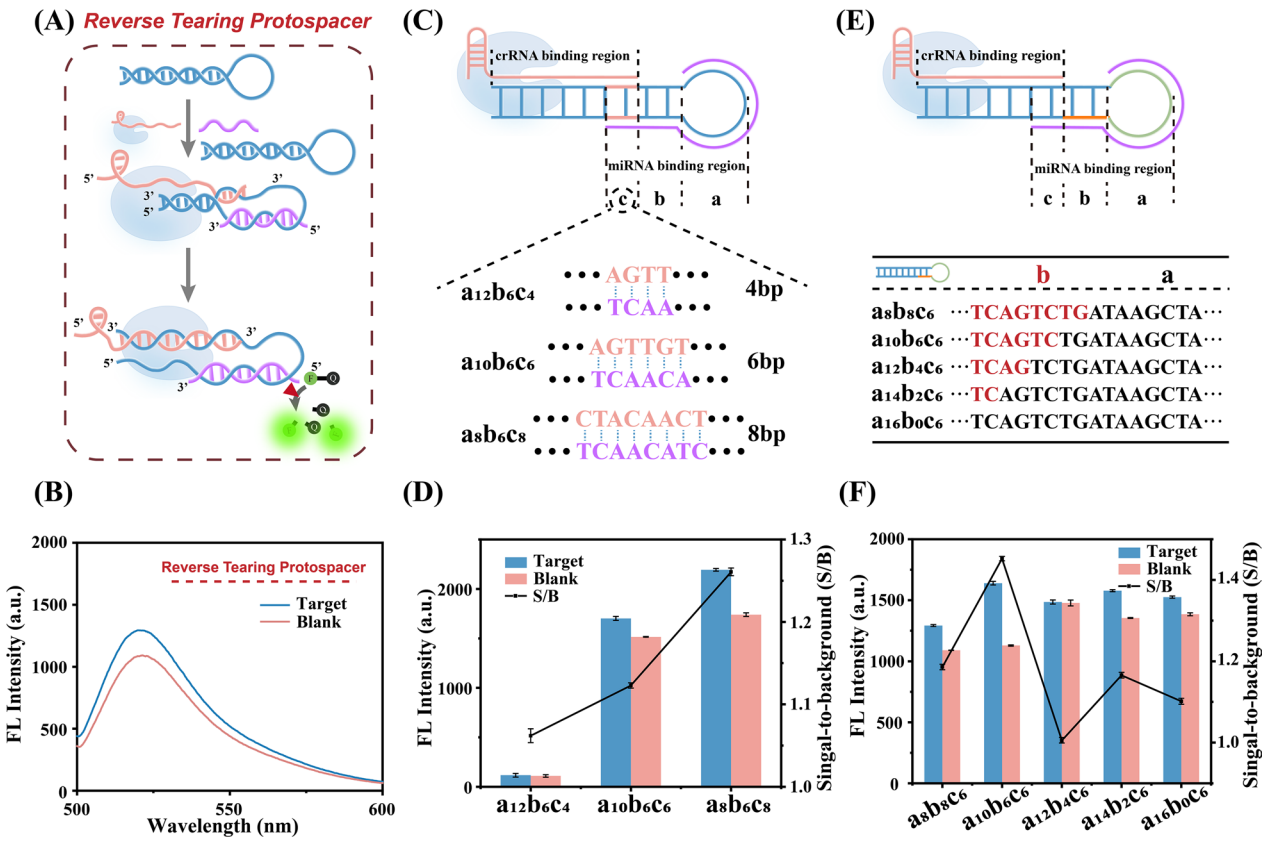

Fig. 2 **A** Schematic illustration and **B** feasibility of TRHDA-based reverse tearing protospacer activated Cas12a. **C** Schematic diagram and **D** optimization of the base pair numbers in the "c" region of hairpin DNA. **E** Schematic diagram and **F** parallel optimization of the base pair numbers in "a" region and "b" region of hairpin DNAs. The data error bars indicate mean ± SD ($n = 3$)

by Amberff14sb force field. Secondary structures of RNA and DNA were generated using the mFold web server, followed by three-dimensional structure prediction with RNAComposer, and parameterization with OL3 and 15 force fields for RNA and DNA, respectively. The likely binding modes of five hairpin DNAs on Cas12a-crRNA-miRNA complex were explored by HDOCK and the best docking model was used for further molecular dynamics simulation and results were visualized by UCSF ChimeraX. A cubic box was established by extending at least 1.4 nm outward along complex ($15\times15\times15$ nm^3). The system was solvated in TIP3P water, and then 0.05 M NaCl and 0.01 M $MgCl_2$ were added to keep it electrically neutral. Energy minimization was performed using the steepest descent algorithm with a force tolerance of 500 kJ·mol^{-1}·nm^{-1}. In all three directions, periodic boundary conditions were imposed. Then system was relaxed for 1 ns under NPT ensemble and position restraints with a constant of 1000 kJ·mol^{-1}·nm^{-2} in three directions were performed on heavy atoms of protein and nucleic acid. After completing the above steps, 100 ns NPT MD simulation was performed. Pressure was maintained at 1 bar by the Parrinello-Rahman barostat in an isotropic manner, and temperature was maintained at 310 K by the V-rescal thermostat, respectively. The LINCS algorithm was performed to constrain the bond lengths of hydrogen atoms. Lennard–Jones interactions were calculated within a cutoff of 1.2 nm, and electrostatic interactions beyond 1.2 nm were treated with the particle-mesh Ewald method with a grid spacing of 0.16 nm. Additionally, the binding free energy of Cas12a-crRNA-miRNA complex and hairpin DNA was analyzed according to MM/PBSA method by gmxMMPBSA tool.

Results and discussion

Design and optimization of TRHDA for tearing protospacer activated Cas12a

As crRNA might bind with the hairpin DNA from two opposite orientations, forward tearing protospacer (identical to crRNA scaffold, Fig. 1A) and reverse tearing protospacer (opposite to crRNA scaffold, Fig. 2A) are designed to activate Cas12a, respectively. Firstly, the feasibility of the forward tearing protospacer activated Cas12a is verified by fluorescence analysis. As shown in

Fig. 1B, in the presence of target miRNA, the fluorescence signal is seven times higher than the blank control (blue curve *vs.* red curve). This result demonstrates that forward tearing protospacer could enable Cas12a activation. To explore the effect of target-responsive hairpin DNA length on forward tearing protospacer activated Cas12a, a series of hairpin DNAs with different base pairs in the tail region are designed (Fig. 1C). Figure 1D demonstrates that there is a significant decrease in signal-to-background (S/B) ratios with the increasing base pair numbers (0, 3 bp, 6 bp). Consequently, it is not recommended to introduce additional base pairs in the tail region of the hairpin DNA. The region where the hairpin DNA hybridized with the target miRNA encompasses three distinct regions: a toehold region marked as "A", a transition region marked as "B", and a seed region marked as "C" (Fig. S1), and the lengths of the above three regions have also been optimized. It is reported that seed region is important for crRNA spacer to bind to protospacer for subsequent Cas12a activation, thus the length of "C" region is firstly investigated [37–39]. As shown in Fig. 1E, a series of hairpin DNAs with different base pairs including 4 bp, 6 bp, and 8 bp in the "C" region are conceived. The results suggest that hairpin DNA with 6 bp of "C" region exhibits the highest S/B ratio, thereby establishing the length of the "C" region at 6 bp for subsequent optimization (Fig. 1F). In addition, the 8 bp hairpin possesses a distinct background signal, which is hypothesized to be caused by a suboptimal PAM sequence (TCTG) in the stem segment of this hairpin [40]. Considering the fixed sequence of miRNA binding region, the "A" region and "B" region of hairpin DNA should be parallel optimized. Specifically, nine hairpin DNAs (H1, H2, H3, H4, H5, H6, H7, H8, and H9) with different base pairs in the "A" region and "B" region are synthesized (Fig. 1G). It could be seen that H5 ($A_{12}B_4C_6$) with 12 bp of "A" region and 4 bp of "B" region represents the highest S/B ratio (Fig. 1H).

Molecular dynamics simulations are implemented to survey the process that Cas12a-crRNA-miRNA complex bond with representative five hairpin DNAs (H1, H3, H5, H7, and H9) and calculate the corresponding binding free energies (Fig. 1I). Remarkably, H5 presents the highest free energy change ($-\Delta G = 363.72$ kJ·mol^{-1}) among the five hairpin DNAs and the change trend of the binding free energies from H1 to H9 is well matched with the change trend of fluorescence signal (Fig. 1J). These results reveal that the process forming the complex of Cas12a-crRNA-miRNA-hairpin DNA may determine the reaction kinetics of the cleavage activities.

Moreover, the reverse tearing protospacer activated Cas12a is also discussed and the schematic illustration of reverse tearing protospacer mode is shown in Fig. 2A. Fluorescence analysis is employed to explore the feasibility of the reverse tearing protospacer activated Cas12a. As presented in Fig. 2B, in the presence of target miRNA, the fluorescence signal is slightly higher than the blank control (blue curve *vs.* red curve), manifesting that reverse tearing protospacer is not conducive to Cas12a activation. Similarly, the region where the hairpin DNA hybridized with the target miRNA is divided into three distinct regions: a toehold region marked as "a", a transition region marked as "b", and a seed region marked as "c" and the lengths of the above three regions have also been optimized. Firstly, three hairpin DNAs are designed, each containing base pairs of 4 bp, 6 bp, and 8 bp in the "c" region (Fig. 2C). Unfortunately, it indicates that all three hairpin DNAs, which has different base pairs in the "c" region, exhibit a low S/B ratio of approximately 1.0 (Fig. 2D). Subsequently, the "a" region and "b" region of hairpin DNA are parallel optimized under "c" region of 6 bp (Fig. 2E). Regretfully, Fig. 2F reveals that all five hairpin DNAs with distinct base pairs in the "a" region and "b" region also exhibit a relatively low S/B ratio of approximately 1.2. These indicate that reverse tearing protospacer activated Cas12a is unavailable.

Based on the above findings, forward tearing protospacer activated Cas12a with $A_{12}B_4C_6$ hairpin DNA as an optimal TRHDA is chosen in the subsequent experiments.

Feasibility of TRHDA-mediated Cas12a for miRNA analysis

The upregulation of miR-21 has been observed in various cancer types and is implicated in tumorigenesis, making it a highly promising biomarker for cancer diagnosis [41, 42]. Therefore, miR-21 is selected as target model to evaluate the feasibility of the TRHDA-mediated Cas12a-powered biosensing. As the proof of the principle, miR-21 binds to the optimal hairpin DNA ($A_{12}B_4C_6$) facilitating the complementarity between crRNA spacer and protospacer in the stem sequence of $A_{12}B_4C_6$, thereby activating the trans-cleavage activity of Cas12a. To validate this design, the PAGE experiment is conducted. As shown in Fig. S2, compared to un-cleaved ssDNA (reporter 2) band in lane 5, the ssDNA (reporter 2) band disappears in lane 6 when miR-21 is added into the mixture of Cas12A-crRNA and hairpin DNA of $A_{12}B_4C_6$. This observation confirms that miR-21 binding to $A_{12}B_4C_6$ could activate the trans-cleave activity of Cas12a through forward tearing protospacer behavior. Next, the reaction rates of ssDNA activator, dsDNA activator and the TRHDA-mediated Cas12a system were investigated through fluorescence kinetic analysis. By further derivation of the fluorescence kinetic curve to obtain the rate curves, it was determined that ssDNA activator has the highest maximum reaction rate, followed by TRHDA-mediated Cas12a system, with dsDNA activator being the slowest.

Of note, the reaction rate of TRHDA-mediated Cas12a system is about twice that of traditional PAM-dependent dsDNA activator (Fig. S3).

Optimization of experimental conditions

To achieve optimal analytical performance for miRNA detection, several experimental conditions such as the reaction temperature of TRHDA-mediated Cas12a system, the concentration of Cas12a-crRNA complex, the type of reaction buffer, and the concentration of $A_{12}B_4C_6$ are optimized. Firstly, the TRHDA-mediated Cas12a system is conducted at various reaction temperatures, namely 25 ℃, 33 ℃, 37 ℃, and 41 ℃. As depicted in Fig. S4, with the increase of reaction temperatures, the S/B ratio increases and achieves its peak at 37 ℃, so 37 ℃ is ultimately chose as the optimal reaction temperature for subsequent experiments. Then, a series of concentrations of Cas12a-crRNA complex are explored to obtain the optimum cleavage activity of Cas12a. As shown in Fig. S5, the concentration of Cas12a-crRNA complex is studied from 10 to 100 nM. The S/B ratio undergoes an upward trend from 10 to 50 nM. After that, S/B ratio dramatically decreases. Therefore, 50 nM is selected as the optimal concentration of Cas12a-crRNA complex in the subsequent research. It is well-known that enzymatic reactions may be significantly affected by reaction buffers. Therefore, the trans-cleavage activity of TRHDA-mediated Cas12a system reacted in NEBuffer r2.1, NEBuffer 3, NEBuffer 4, and rCutsmart buffer is investigated, respectively. As illustrated in Fig. S6, although the highest fluorescence signal is observed in NEBuffer 4, it has a relatively high background signal. Obviously, the highest S/B ratio is received in NEBuffer 3, which is selected to utilize in follow-up experiments. As everyone knows, the activated Cas12a could indiscriminately trans-cleavage ssDNA, which causes that the loop of hairpin $A_{12}B_4C_6$ and the F-Q reporter could be trans-cleaved in this system. If the concentration of hairpin $A_{12}B_4C_6$ is excess, the excessive hairpin $A_{12}B_4C_6$ could compete with F-Q reporter to be trans-cleaved by activated Cas12a, resulting in signal inhibition. Thus, we optimize the concentration of hairpin $A_{12}B_4C_6$ to improve the detection performance and results are depicted in Fig. S7. The hairpin $A_{12}B_4C_6$ concentration-dependent S/B ratio increases till it reaches highest peak at 25 nM, indicating that 25 nM of hairpin $A_{12}B_4C_6$ is enough to guarantee the target miRNA binding for subsequent reaction. After that, the S/B ratio gradually decreases, which is attributed to the hairpin $A_{12}B_4C_6$ is competitive with F-Q reporter to be non-specifical trans-cleavage by Cas12a. Therefore, the favorable concentration of the hairpin $A_{12}B_4C_6$ at 25 nM is adopted in the following experiments.

Analytical performance of TRHDA-mediated Cas12a system for universal miRNA assay

As a proof-of-concept TRHDA-mediated Cas12a system, the designed input-responsive hairpin DNA contains the specific target miRNA binding site, which further engineers different hairpin DNAs for universal miRNA detection (Fig. 3A). Here, three hairpin DNAs ($A_{12}B_4C_6$) with distinct sequences are constructed to individually detect miR-21, let-7a, and miR-30a under the optimized experimental conditions. Figure 3B shows that the fluorescence intensities are increased with the increasing target miR-21 concentrations in the range of 50 pM-15 nM. In addition, the ΔFluorescence intensity ($F\text{-}F_0$), which is the difference in fluorescence intensity between the target miRNA and blank, represents a good linear relationship over the dynamic range of 50 pM to 15 nM. The correction equation is $\Delta F = 640.60C + 207.95$ with the correlation coefficient (R^2) of 0.9766 (Fig. 3C). The limit of detection (LOD) is calculated to be 13.9 pM according to the rule of 3 times standard deviation over the blank response. Furthermore, the developed TRHDA mediated Cas12a-powered method for miR-21 detection has been compared to other reported sensing assays in terms of linearity and LOD. As shown in Table S2, the designed miR-21 biosensing method has a satisfactory analytical performance, which is attributed to exceptional trans-cleavage activity of TRHDA-mediated Cas12a as a signal amplifier.

Selectivity is equally important to the proposed fluorescent assay for miRNA detection. To explore the selectivity of the approach for miR-21 analysis, a variety of cancer-associated miRNAs, including miR-122, miR-141, miR-155, miR-378, and let-7a, are added to the detection system, each at the concentration of 10 nM. Weak fluorescence signals are observed in the presence of the interfering miRNAs, which is approximate to the signal of blank control. However, when miR-21 is present alone or together with the other five interfering miRNAs, a strong fluorescence signal is obtained (Fig. 3D). These results validate that target-binding driven forward tearing protospacer behavior to activate cleavage activities of TRHDA-mediated Cas12a, thereby ensuring the high selectivity of the proposed method for miR-21 detection.

Meanwhile, the TRHDA-mediated Cas12a-powered methods for sensitivity and selectivity of general detection of let-7a and miR-30a are also investigated. For both target let-7a and miR-30a, the fluorescence intensities are in line with the law that miRNA concentration is proportional from 100 pM to 15 nM (Fig. 3E and H). As displayed in Fig. 3F and I, their correction equations for let-7a and miR-30a detection are $\Delta F = 551.63\ C + 351.42$ with the correlation coefficient (R^2) of 0.9683 and $\Delta F = 500.52\ C + 234.83$ with the correlation coefficient

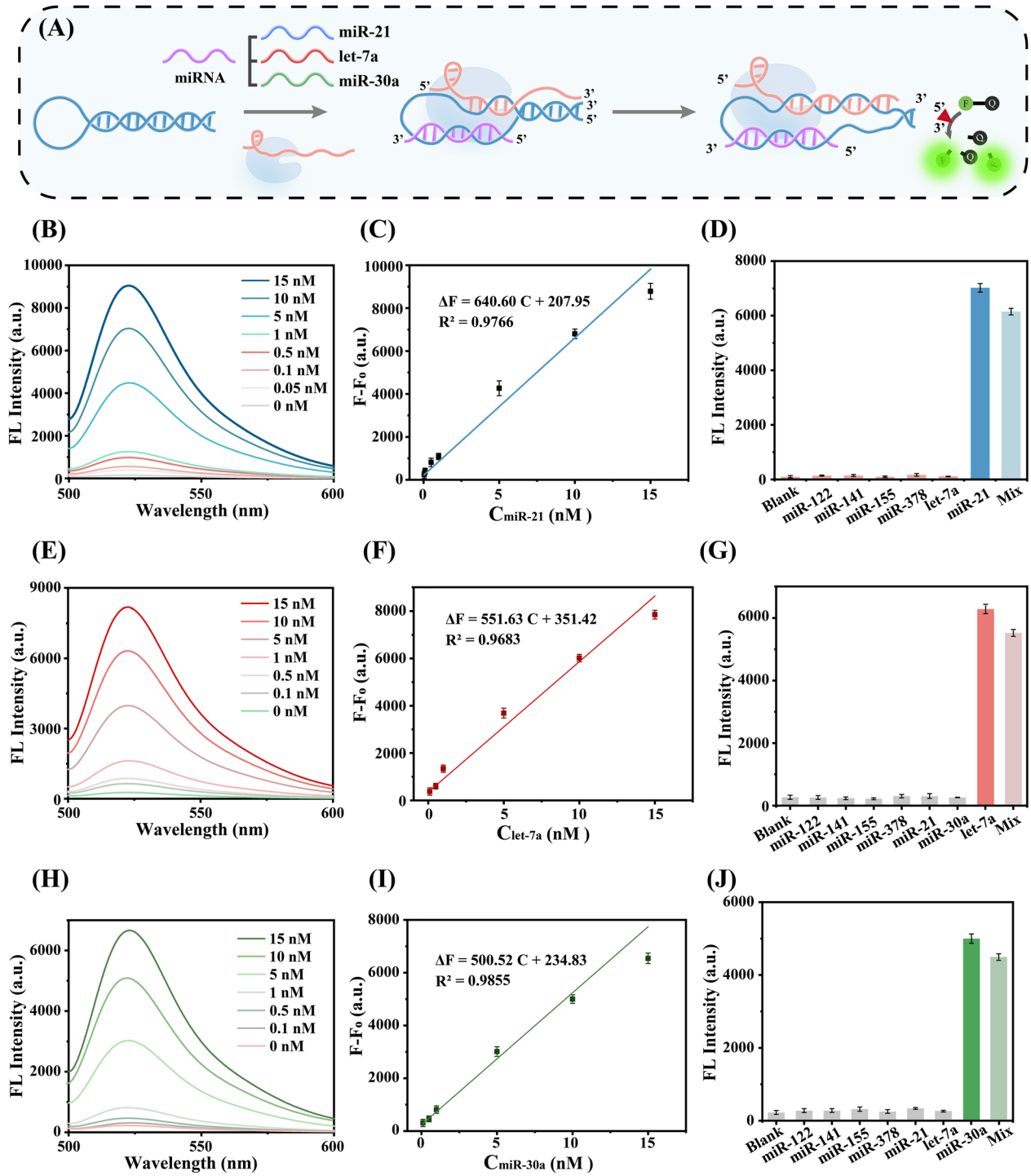

Fig. 3 Analytical performance of TRHDA-mediated Cas12a-powered universal assays for three different miRNAs (miR-21, let-7a, and miR-30a) detection. **A** Principle diagrams of universal assays for miR-21, let-7a, and miR-30a detection with TRHDA-mediated Cas12a system. Fluorescence spectrum showing different concentrations of **B** miR-21 (0.05–15 nM), **E** let-7a (0.1–15 nM), and **H** miR-30a (0.1–15 nM). Linear relationship between the fluorescence intensity and **C** miR-21 concentration in the range of 0.05–15 nM, **F** let-7a concentration in the range of 0.1–15 nM, **I** miR-30a concentration in the range of 0.1–15 nM. Selectivity of the TRHDA-mediated Cas12a based assays for **D** miR-21 detection, **G** let-7a detection, and **J** miR-30a detection against the interference miRNAs and a blank control. The data error bars indicate mean ± SD ($n = 3$)

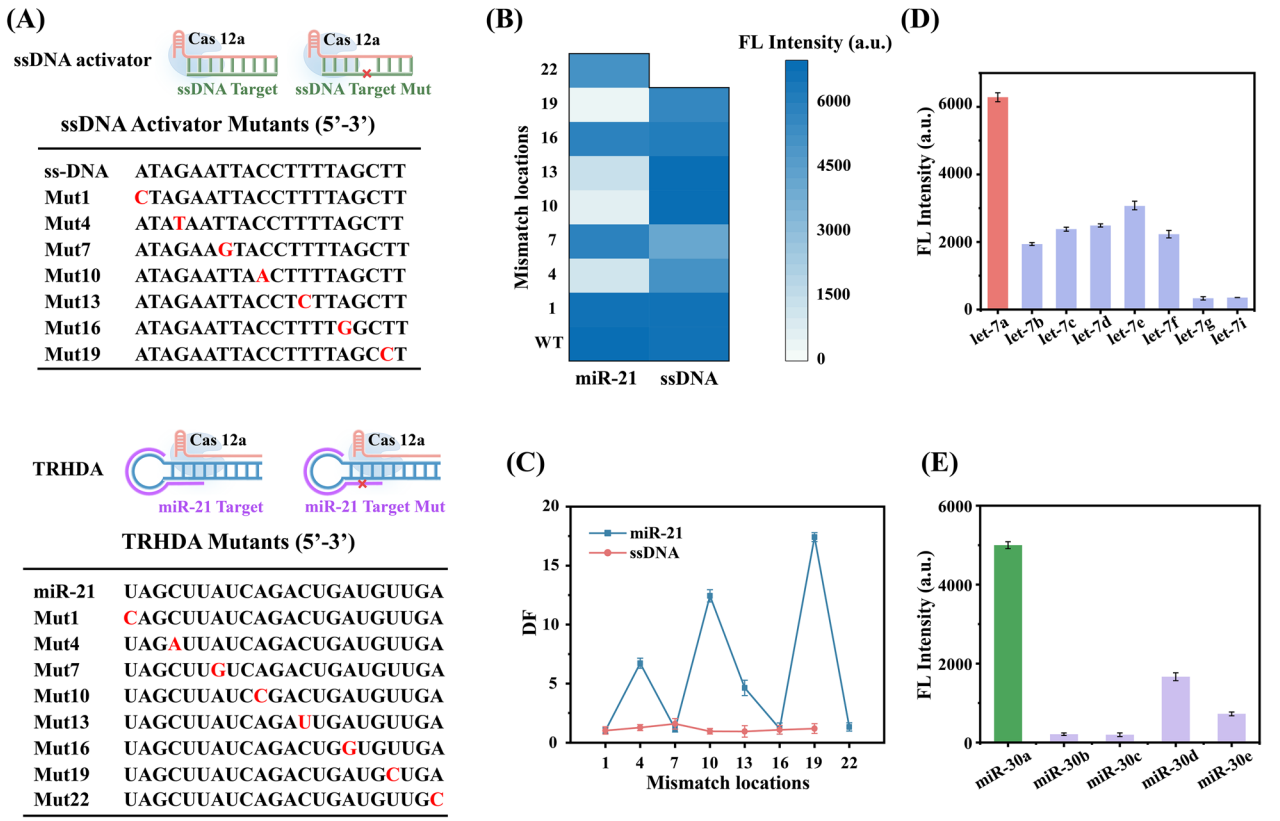

Fig. 4 **A** Schematic of ssDNA activator *vs.* TRHDA for the detection of a target nucleic acid. SsDNA activator and miR-21 are designed with single-base mutations across the length of the activator. The mutation location is identified by 'Mut' following the nucleotide number where the base has been changed. **B** The heat map represents the fluorescence intensity of different mutation activators. **C** Comparison of DF of ssDNA activators and TRHDA containing different single-base mutations in different positions. **D** Fluorescence signals of different members of the let-7 family. **E** Fluorescence signals of different members of the miR-30 family. The data error bars indicate mean ± SD ($n = 3$)

(R^2) of 0.9855, respectively. According to the 3-times standard deviation of the blank response, the LODs of let-7a and miR-30a detection are calculated to be 26.6 pM and 32.4 pM, respectively. Similarly, several irrelevant interfering miRNAs are used to estimate the selectivity of the proposed methods for let-7a and miR-30a detection. In Fig. 3G and J, the fluorescence signals of nonspecific groups closely resemble the blank control, whereas the addition of target let-7a or miR-30a only induces a strong fluorescence signal. These findings demonstrate that the proposed methods effectively discriminate miRNAs based on the well-design of target-responsive hairpins in the TRHDA.

Identification of single-base mismatches and homologous miRNA family in TRHDA-mediated Cas12a activation mode

The ability to distinguish single-base mismatches and highly homologous miRNA families poses a significant challenge in clinical molecular diagnostics. To investigate the discrimination of single-base mutations by the designed TRHDA-mediated Cas12a activation mode in targets compared to ssDNA activation mode, we introduce single-point mutations into miR-21 and ssDNA activator to activate Cas12a for comparison (Fig. 4A). The specificity of two activators-mediated Cas12a activation modes is evaluated by the discrimination factor (DF) which is calculated using formula (1).

$$\mathrm{DF} = \frac{\mathrm{RFU}_{[\mathrm{Target}]}}{\mathrm{RFU}_{[\mathrm{Target\ Mut}]}} \tag{1}$$

where $\mathrm{RFU}_{[\mathrm{Target}]}$ means the fluorescence intensity for ssDNA target or miR-21 target and $\mathrm{RFU}_{[\mathrm{Target\ Mut}]}$ means the fluorescence intensity for ssDNA target mutant or miR-21 target mutant. As depicted in Fig. 4B and C, it is observed that all ssDNA activators in positions Mut1-Mut19 are able to activate Cas12a, indicating that the

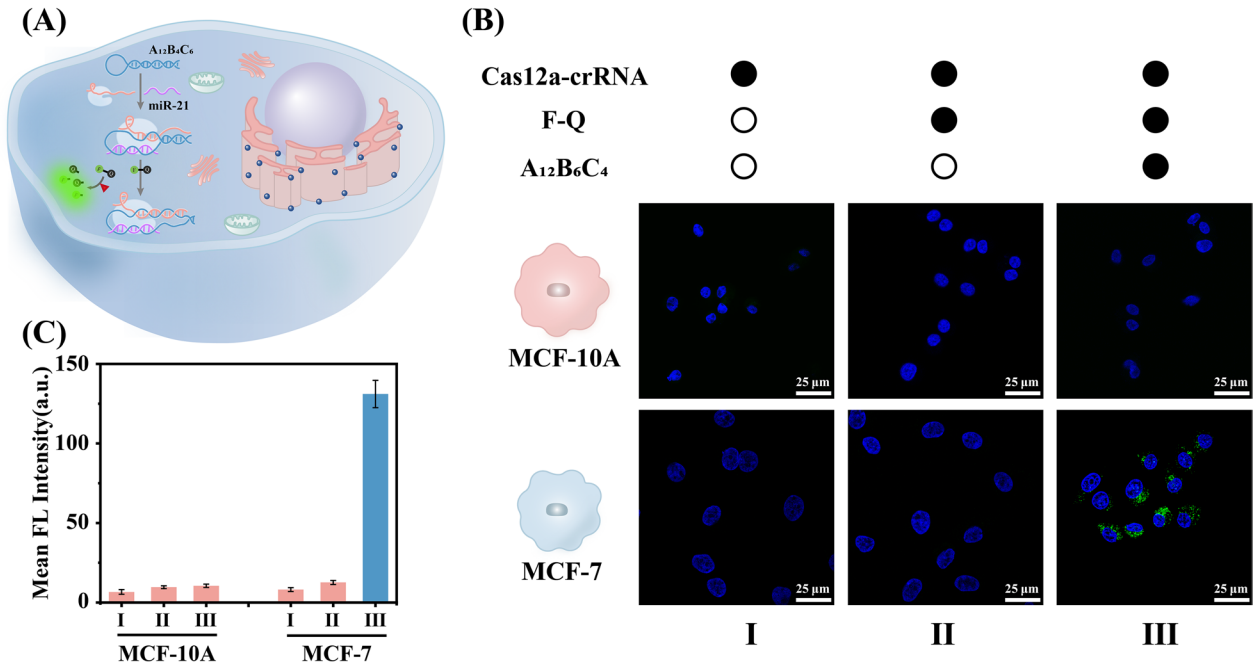

Fig. 5 The TRHDA-mediated Cas12a sensing of miRNA in cells. **A** Schematic illustration of TRHDA-mediated Cas12a system for miR-21 imaging in cell. **B** Confocal microscopic images and **C** the corresponding fluorescence intensities of each cell with different treatments. The scale bar is 25 μm. The data error bars indicate mean ± SD ($n = 3$)

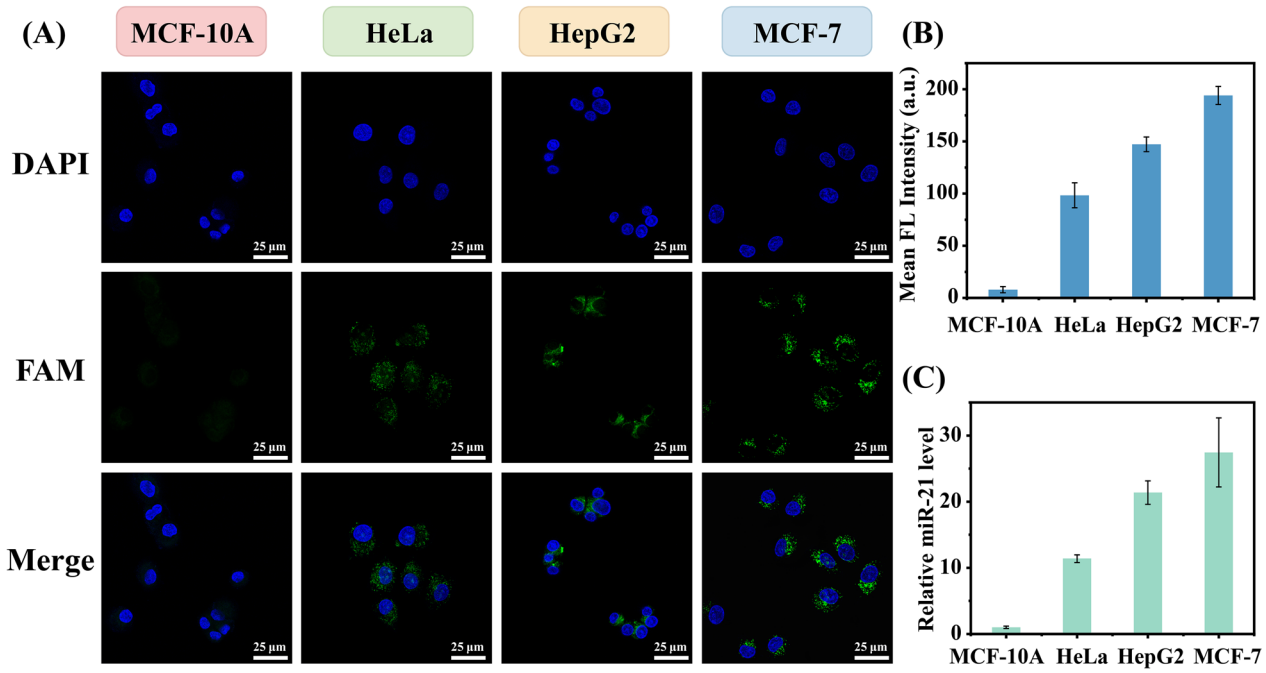

Fig. 6 **A** Confocal microscopic images and **B** the corresponding fluorescence intensities of TRHDA-mediated Cas12a system for miR-21 imaging in MCF-10A, HeLa, HepG2, and MCF-7 cells. The mean fluorescence intensities of the corresponding groups ($n = 3$) are displayed in histograms. **C** The qRT-PCR results of the relative miR-21 expression levels in MCF-10A, HeLa, HepG2, and MCF-7 cells. The scale bar is 25 μm. The data error bars indicate mean ± SD ($n = 3$)

ability of ssDNA activation mode to distinguish single-base mutations is relatively poor, which is consistent with the previous works [23]. However, miR-21 mutations in positions Mut4, Mut10, Mut13, and Mut19 significantly reduce the trans-cleavage activity of TRHDA-mediated Cas12a, suggesting the differentiation of single-base mutations in TRHDA is location-dependent. Clearly, compared to traditional ssDNA activators, TRHDA-mediated Cas12a activation mode exhibits improved discriminatory capacity for target mutations, as expected.

To further assess the specificity of the designed TRHDA-mediated Cas12a activation mode in miRNA assays, we utilize let-7 family and miR-30 family as model targets, which exhibit high sequence homology and some of them even differing by only one base. In Fig. 4D, it is evident that the fluorescence signal of let-7a surpass that of other let-7 members significantly. Notably, even the most indistinguishable let-7c, let-7e, and let-7f could be distinguished from let-7a. Similarly, in Fig. 4E, the fluorescence signal of miR-30a exhibits superiority over other miR-30 members. These findings elucidate that the designed TRHDA demonstrates exceptional specificity when dealing with highly homologous miRNA families.

Intracellular imaging of miR-21 via TRHDA-mediated Cas12a system

Benefiting from the excellent in vitro analytical performance of the designed TRHDA-mediated Cas12a sensing for miRNA detection, the applicability of TRHDA-mediated Cas12a system for miR-21 intracellular imaging is further explored (Fig. 5A). Here, MCF-7 cell line with high expression levels of miR-21 and MCF-10A cell line with low expression levels of miR-21 are used for intracellular imaging. To demonstrate the capability of TRHDA-mediated Cas12a system for miR-21 sensing in cells, the two cell lines (MCF-7 and MCF-10A) are treated with three experimental conditions (group I: only Cas12a-crRNA, group II: Cas12a-crRNA and F-Q reporter, group III: all of Cas12a-crRNA, F-Q reporter and hairpin $A_{12}B_4C_6$) in parallel, respectively. As shown in Fig. 5B, no significant green fluorescence in the MCF-10A cells is observed in the three groups. Besides, no green fluorescence in the MCF-7 cells is observed in the two control groups (group I and II), whereas bright green fluorescence in the MCF-7 cells is observed in experimental group (group III), as expected. The corresponding fluorescence intensity quantified by Image J software is evaluated in Fig. 5C. These results suggest that the strong green fluorescence is caused by target miR-21 binding to TRHDA to activate the Cas12a for cleaving F-Q reporter, rather than by non-specific degradation of the F-Q reporter.

Considering the differential expression levels of miRNA in various cellular contexts, it is imperative to assess the applicability of TRHDA-mediated Cas12a sensing for visualizing miR-21 in alternative cells, including MCF-7 cells, HepG2 cells, HeLa cells, and MCF-10A. The fluorescence images in Fig. 6A clearly demonstrate distinct green fluorescence observed in MCF-7, HepG2, and HeLa cells. Conversely, MCF-10A cells exhibit minimal green fluorescence. The quantification of mean fluorescence intensities for four distinct cell types in Fig. 6B demonstrates a sequential increase in fluorescence intensity, highlighting the robust capability of the TRHDA-mediated Cas12a system to detect miR-21 across various tumor cell lines. To further illustrate the strong correlation between FAM fluorescence intensity and miR-21 expression, we conduct qRT-PCR analysis to examine the expression levels of miR-21 in above-mentioned cell lines. Remarkably, the results are in complete concordance with those yielded by the designed TRHDA-mediated Cas12a sensing assay (Fig. 6B vs. C). Collectively, these findings unequivocally demonstrate that the proposed TRHDA-mediated Cas12a sensing holds immense potential for detecting endogenous miRNAs within cells.

Conclusions

In summary, the engineered target-responsive hairpin DNA activator (TRHDA) has been developed to regulate forward tearing protospacer activated CRISPR-Cas12a system, enabling direct miRNA detection with high specificity and sensitivity. Specifically, the reconfiguration of hairpin DNA induced by target binding serves as the driving force for tearing protospacer in the stem of hairpin DNA, thereby enabling the complementarity between crRNA spacer and protospacer to activate Cas12a. Considering the specificity and sensitivity of Cas12a-powered biosensing for miRNA detection, the optimal structure of hairpin DNA has been investigated by fluorescence analysis and molecular dynamics simulations. Upon the optimal hairpin DNA as input-responsive activator of Cas12a, we present a universal detection method for different miRNAs (miR-21, let-7a, miR-30a) with low LODs (13.9 pM, 26.6 pM, 32.4 pM, respectively) and excellent capability in identifying single-base mismatches and homologous miRNA families. Furthermore, TRHDA-mediated Cas12a based miR-21 biosensing strategy enables the evaluation of miRNA expression levels in diverse cellular contexts by intracellular imaging, which offers

significant implications for molecular diagnostics utilizing the CRISPR-Cas12a system toolbox.

Supplementary Information

The online version contains supplementary material available at https://doi.org/10.1186/s12951-024-02915-5.

Additional file 1: Materials and reagents, apparatus, preliminary analysis in serum samples. **Table S1**: Sequences of nucleic acids used in this work. **Fig. S1**: The sequence illustration of hairpin DNA as a bridge linking miRNA recognition and Cas12a activation. **Fig. S2**: PAGE analysis of TRHDA-mediated CRISPR-Cas12a system for miR-21 detection. **Fig. S3**: Comparison of the reaction rates of Cas12a activated by ssDNA activator, dsDNA activator and the designed TRHDA. **Fig. S4**: Optimization of reaction temperature of TRHDA-mediated Cas12a system. **Fig. S5**: Optimization of Cas12a-crRNA concentration in the TRHDA-mediated Cas12a system. **Fig. S6**: Optimization of buffer type in the TRHDA-mediated Cas12a system. **Fig. S7**: Optimization of hairpin concentration in the TRHDA-mediated Cas12a system. **Table S2:** Performance comparison of this method and the reported methods for miR-21 detection. **Table S3:** The proposed biosensor for the determination of miR-21 in patient serum samples. **Fig. S8**: Exploring the incubation time of TRHDA-mediated Cas12a in cell imaging. **Fig. S9**: Exploring the concentration of TRHDA-mediated Cas12a system in cell imaging.

Acknowledgements
This research was supported by the National Natural Science Foundation of China (82272431, 22204014), Chongqing Natural Science Foundation Innovation and Development Joint Fund (CSTB2022NSCQ-LZX0046), Postdoctoral Natural Science Foundation of Chongqing (CSTB2022NSCQ-BHX0008). Science and Technology Research Program of Chongqing Municipal Education Commission (KJQN202300443). Min Zhao is supported by Chongqing Bayu Young Scholar program.

Author contributions
LZ, XD performed all experimental work. YL, QZ, LX, and JX conducted data analysis. AC, WC and MZ revised the manuscript and provided project guidance. AC and MZ procured funding and data curation. All authors read and approved the final manuscript." to "LZ and XD performed the experiments, analyzed data and wrote the manuscript. YL, QZ and LX conducted data analysis. JX and WC provided project guidance. AC and MZ designed the study, guided the experiments, analyzed and interpreted data, and revised this manuscript. All authors read and approved the final manuscript.

Availability of data and materials
No datasets were generated or analysed during the current study.

Declarations

Consent for publication
All authors have provided consent for the manuscript to be published.

Competing interests
The authors declare no competing interests.

Author details
[1]Key Laboratory of Clinical Laboratory Diagnostics (Ministry of Education), College of Laboratory Medicine, Chongqing Medical University, Chongqing 400016, China. [2]Department of Clinical Laboratory, University-Town Hospital of Chongqing Medical University, Chongqing 401331, China. [3]School of Public Health, Chongqing Medical University, Chongqing 400016, China. [4]The Center for Clinical Molecular Medical Detection, The First Affiliated Hospital of Chongqing Medical University, Chongqing 400042, China.

Received: 17 June 2024 Accepted: 9 October 2024
Published online: 08 November 2024

References

1. Breulmann FL, Hatt LP, Schmitz B, Wehrle E, Richards RG, Della Bella E, et al. Prognostic and therapeutic potential of microRNAs for fracture healing processes and non-union fractures: a systematic review. Clin Transl Med. 2023;13: e1161.
2. Wang L, Liu LZ, Jiang BH. Dysregulation of microRNAs in metal-induced angiogenesis and carcinogenesis. Semin Cancer Biol. 2021;76:279–86.
3. Rashed WM, Hamza MM, Matboli M, Salem SI. MicroRNA as a prognostic biomarker for survival in childhood acute lymphoblastic leukemia: a systematic review. Cancer Metastasis Rev. 2019;38:771–82.
4. Yan J, Zhong X, Zhao Y, Wang X. Role and mechanism of miRNA in cardiac microvascular endothelial cells in cardiovascular diseases. Front Cardiovasc Med. 2024;11:1356152.
5. Pasławska M, Grodzka A, Peczyńska J, Sawicka B, Bossowski AT. Role of miRNA in cardiovascular diseases in children-systematic review. Int J Mol Sci. 2024;25:956.
6. Lozano-Velasco E, Inácio JM, Sousa I, Guimarães AR, Franco D, Moura G, et al. miRNAs in heart development and disease. Int J Mol Sci. 2024;25:1673.
7. Yu S, Wang H, Liu T, Liang C, Luo J. A knowledge-driven network for fine-grained relationship detection between miRNA and disease. Brief Bioinform. 2022;23:bbac058.
8. Jet T, Gines G, Rondelez Y, Taly V. Advances in multiplexed techniques for the detection and quantification of microRNAs. Chem Soc Rev. 2021;50:4141–61.
9. Dave VP, Ngo TA, Pernestig AK, Tilevik D, Kant K, Nguyen T, et al. MicroRNA amplification and detection technologies: opportunities and challenges for point of care diagnostics. Lab Invest. 2019;99:452–69.
10. Kilic T, Erdem A, Ozsoz M, Carrara S. MicroRNA biosensors: opportunities and challenges among conventional and commercially available techniques. Biosens Bioelectron. 2018;99:525–46.
11. Forero DA, González-Giraldo Y, Castro-Vega LJ, Barreto GE. qPCR-based methods for expression analysis of miRNAs. Biotechniques. 2019;67:192–9.
12. Muthamilselvan S, RamasamiSundharBaabu P, Palaniappan A. Microfluidics for profiling miRNA biomarker panels in AI-assisted cancer diagnosis and prognosis. Technol Cancer Res Treat. 2023;22:15330338231185284.
13. Xu H, Wu X, Liu Q, Yang C, Shen M, Wang Y, et al. A universal strategy for enhancing the circulating miRNAs' detection performance of rolling circle amplification by using a dual-terminal stem-loop padlock. ACS Nano. 2024;18:436–50.
14. Zhou S, Liu M, Deng L, Qiu Y, Gu T, Chen J, et al. Double CRISPR/Cas12a-drived hyperbranched rolling circle amplification with triple signal amplification enables low background miRNA detection. Sensor Actuat B-Chem. 2024;408: 135490.
15. Dai W, Zhang J, Meng X, He J, Zhang K, Cao Y, et al. Catalytic hairpin assembly gel assay for multiple and sensitive microRNA detection. Theranostics. 2018;8:2646.
16. Zhang Y, Sun M, Xie J, Chen J, Huang T, Duan WJ, et al. Dual-signal amplification strategy based on catalytic hairpin assembly and APE1-assisted amplification for high-contrast miRNA imaging in living cells. Anal Chem. 2024;96:910–6.
17. Cao D, Qin X, Wang W, Zhang Y, Peng S, Gong H, et al. Designing a hybrid chain reaction probe for multiplex transcripts assay with high-level imaging. ACS Nano. 2024;18:618–29.
18. Li R, Li F, Zhang Y, He Y, Wang Y, Wang F. Miniature hierarchical DNA hybridization circuit for amplified multiplexed MicroRNA imaging. Anal Chem. 2023;95:3848–55.
19. Jinek M, Chylinski K, Fonfara I, Hauer M, Doudna JA, Charpentier E. A programmable dual-RNA-guided DNA endonuclease in adaptive bacterial immunity. Science. 2012;337:816–21.
20. Tao J, Bauer DE, Chiarle R. Assessing and advancing the safety of CRISPR-Cas tools: from DNA to RNA editing. Nat Commun. 2023;14:212.
21. Kaminski MM, Abudayyeh OO, Gootenberg JS, Zhang F, Collins JJ. CRISPR-based diagnostics. Nat Biomed Eng. 2021;5:643–56.
22. Hong J, Son T, Castro CM, Im H. CRISPR/Cas13a-based MicroRNA detection in tumor-derived extracellular vesicles. Adv Sci. 2023;10:2301766.
23. Chen JS, Ma E, Harrington LB, Da Costa M, Tian X, Palefsky JM, et al. CRISPR-Cas12a target binding unleashes indiscriminate single-stranded DNase activity. Science. 2018;360:436–9.

24. Gootenberg JS, Abudayyeh OO, Lee JW, Essletzbichler P, Dy AJ, Joung J, et al. Nucleic acid detection with CRISPR-Cas13a/C2c2. Science. 2017;356:438–42.
25. Li SY, Cheng QX, Wang JM, Li XY, Zhang ZL, Gao S, et al. CRISPR-Cas12a-assisted nucleic acid detection. Cell Discov. 2018;4:20.
26. Stella S, Alcón P, Montoya G. Structure of the Cpf1 endonuclease R-loop complex after target DNA cleavage. Nature. 2017;546:559–63.
27. Deng F, Li Y, Yang B, Sang R, Deng W, Kansara M, et al. Topological barrier to Cas12a activation by circular DNA nanostructures facilitates autocatalysis and transforms DNA/RNA sensing. Nat Commun. 2024;15:1818.
28. Zhang J, Li Z, Guo C, Guan X, Avery L, Banach D, et al. Intrinsic RNA targeting triggers indiscriminate DNase activity of CRISPR-Cas12a. Angew Chem Int Ed. 2024;63:e202403123.
29. Moon J, Liu C. Asymmetric CRISPR enabling cascade signal amplification for nucleic acid detection by competitive crRNA. Nat Commun. 2023;14:7504.
30. Collias D, Vialetto E, Yu J, Co K, Almási ÉDH, Rüttiger A-S, et al. Systematically attenuating DNA targeting enables CRISPR-driven editing in bacteria. Nat Commun. 2023;14:680.
31. Karlikow M, Amalfitano E, Yang X, Doucet J, Chapman A, Mousavi PS, et al. CRISPR-induced DNA reorganization for multiplexed nucleic acid detection. Nat Commun. 2023;14:1505.
32. Zetsche B, Gootenberg JS, Abudayyeh OO, Slaymaker IM, Makarova KS, Essletzbichler P, et al. Cpf1 is a single RNA-guided endonuclease of a class 2 CRISPR-Cas system. Cell. 2015;163:759–71.
33. Guo Z, Tan X, Yuan H, Zhang L, Wu J, Yang Z, et al. Bis-enzyme cascade CRISPR-Cas12a platform for miRNA detection. Talanta. 2023;252: 123837.
34. Peng S, Tan Z, Chen S, Lei C, Nie Z. Integrating CRISPR-Cas12a with a DNA circuit as a generic sensing platform for amplified detection of microRNA. Chem Sci. 2020;11:7362–8.
35. Li QN, Wang DX, Han GM, Liu B, Tang AN, Kong DM. Low-background CRISPR/Cas12a sensors for versatile live-cell biosensing. Anal Chem. 2023;95:15725–35.
36. Feng S, Chen H, Hu Z, Wu T, Liu Z. Ultrasensitive detection of miRNA via CRISPR/Cas12a coupled with strand displacement amplification reaction. ACS Appl Mater Interfaces. 2023;15:28933–40.
37. Stella S, Mesa P, Thomsen J, Paul B, Alcón P, Jensen SB, et al. Conformational activation promotes CRISPR-Cas12a catalysis and resetting of the endonuclease activity. Cell. 2018;175:1856–71.
38. Swarts DC, Jinek M. Mechanistic insights into the cis- and trans-acting DNase activities of Cas12a. Mol Cell. 2019;73:589–600.
39. Chen S, Wang R, Peng S, Xie S, Lei C, Huang Y, et al. PAM-less conditional DNA substrates leverage trans-cleavage of CRISPR-Cas12a for versatile live-cell biosensing. Chem Sci. 2022;13:2011–20.
40. Lu S, Tong X, Han Y, Zhang K, Zhang Y, Chen Q, et al. Fast and sensitive detection of SARS-CoV-2 RNA using suboptimal protospacer adjacent motifs for Cas12a. Nat Biomed Eng. 2022;6:286–97.
41. Lee SH, Brianna. Association of microRNA-21 expression with breast cancer subtypes and its potential as an early biomarker. Pathol Res Pract. 2024;254:155073.
42. Kalariya BJ, RDR AJ, Sumanth S, Guruprasath SA. study on the investigation of the biomarker potential of miRNA-21 expression in colorectal tumor samples and serum. Int Surg J. 2024;11:205–8.

Publisher's Note